

Tailoring optical pulling forces with composite microspheres

R. Ali ^{1,*}, F. A. Pinheiro,¹ R. S. Dutra ², and P. A. Maia Neto¹

¹*Instituto de Física, Universidade Federal do Rio de Janeiro, Caixa Postal 68528, Rio de Janeiro, Rio de Janeiro 21941-972, Brazil*

²*LISComp-IFRJ, Instituto Federal de Educação, Ciência e Tecnologia, Rua Sebastião de Lacerda, Paracambi, Rio de Janeiro 26600-000, Brazil*



(Received 3 June 2020; accepted 16 July 2020; published 10 August 2020)

Optical pulling forces or tractor beams can pull particles against light propagation by redirecting the incident photons forward. This is typically achieved using Bessel beams with very small half-cone angles, which considerably limits their applicability. One can circumvent such an issue by using a superposition of plane waves. In order to investigate optical pulling forces exerted by a pair of noncollinear plane waves, we develop a theoretical framework based on Mie theory, Debye potentials, and Wigner rotation matrices. We apply this framework to calculate the optical pulling force on metalodielectric composite particles, which we put forward as an alternative material platform to optimize and tailor tractor beams. Indeed, we demonstrate that by adding a few plasmonic inclusions to low-refractive-index dielectric particles of arbitrary sizes, we are able to produce polarization-dependent optical pulling forces that cannot occur in the corresponding homogeneous particles. Altogether, our findings not only provide innovative theoretical methods to compute optical pulling forces but also provide strategies to tailor and optimize them, paving the way to increase their applicability.

DOI: [10.1103/PhysRevA.102.023514](https://doi.org/10.1103/PhysRevA.102.023514)

I. INTRODUCTION

Light exerts radiation pressure on matter due to momentum exchange. Focused light beams exert an optical scattering force (forward force due to radiation pressure), as well as a gradient force (possibly along the backward direction) on small particles owing to the inhomogeneity of the electromagnetic field. As an example of application, in optical tweezers a tightly focused beam is used for optical manipulation [1–4] and optical rotation [5–9] with many applications [10–13].

On the other hand, a plane wave will always push a particle made of a passive medium along the forward direction. However, under certain conditions spatially structured beams can accelerate small particles along the direction opposite to the light-propagation direction [14–18]. Negative optical force or optical pulling force (OPF) occurs whenever illuminated particles are pulled towards the source due to the momentum conservation. In contrast to the trapping force in optical tweezers, the OPF can accelerate particles over a long distance without defining an equilibrium position. OPF has attracted considerable attention due to its many applications such as optical sorting [19,20], self-assembling, remote sampling [21,22], miniaturization of nanodevices [23], and enantioselective manipulation [24–29] (see [30] for a recent review). In particular, it was shown both theoretically and experimentally that nondiffracting Bessel beams can pull a subwavelength dielectric sphere [15,22,31]. Several approaches exist to demonstrate OPF on homogeneous dielectric spherical particles using bichromatic fields [32] and multiple plane waves [33,34] and with optical gain [35,36].

OPF can be achieved for weakly absorptive particles that maximize forward scattering while minimizing backward scattering [15,30,33,37]. Typically, it is easier to pull high-refractive-index particles, especially in the size range close to the laser wavelength λ . Particles made of Si, Ge, and GaAs can be pulled even when they are very small, with radii in the range $R \gtrsim 0.2 \lambda$, because of the significant forward scattering and negligible backscattering due to the strong coherent interference between the electric and magnetic dipoles [33,34]. In contrast, particles made of lower-refractive-index materials such as polystyrene and silica can be pulled only for relatively larger radii $R \gtrsim 0.4 \lambda$ [15,22].

The angular distribution of Mie scattering is clearly a key feature to achieve OPF. In that respect, progress in the fields of metamaterials and plasmonics now allows for novel strategies to tailor the interplay between electric and magnetic multipoles to produce directional Mie scattering [15,33,38]. In particular, when considering composite microspheres, it is possible to minimize backscattering by tuning the filling fraction of inclusions [39,40].

In this work we show that metalodielectric composite microspheres, with metallic inclusions embedded in a low-index dielectric host, provide an optimal material platform that allows for pulling forces in a size range well below the laser wavelength, thus extending the applicability domain of OPF towards smaller sizes and lower refractive indexes. Specifically, we put forward a scheme using a superposition of plane waves, in contrast to the traditional approach that employs structured light beams. Our model describes the case of two collimated Gaussian light beams with beam waists much larger than the particle size that thus lead to long-range optical forces. This is typically the case of paraxial beams as we consider sphere radii smaller than or of the order of λ . In order to consider our proposal, we develop an analytical

*rali.physicist@gmail.com

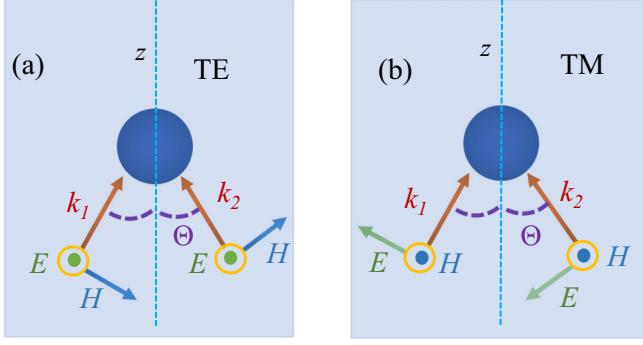


FIG. 1. Schematic diagram of a particle illuminated by two noncollinear plane waves with (a) transverse-electric (TE) and (b) transverse-magnetic (TM) polarization. The angle between the corresponding wave vectors is 2Θ .

framework to compute optical forces based on Mie theory, Debye potentials, and Wigner rotation matrices and apply it to situations such as the one depicted in Fig. 1.

This paper is organized as follows. Section II is devoted to the derivation of our theoretical formalism, which is based on Mie scattering theory combined with Wigner rotations. In Sec. III, we present the numerical results for the OPF on a metallodielectric composite. Finally, we summarize our findings and conclusions in Sec. IV.

II. OPTICAL FORCE EXERTED BY A SUPERPOSITION OF PLANE WAVES ON A MIE SPHERE

In the following we present our theoretical approach to the optical force on a microsphere. We consider a superposition of two linearly polarized noncollinear plane waves, as indicated in Fig. 1. The corresponding wave vectors define the plane shown in Fig. 1, with respect to which we define transverse-electric (TE) and transverse-magnetic (TM) polarizations. We assume that both plane waves are linearly polarized along the same direction. The mixed case or a higher number of plane waves can also be considered within our formalism. In order to allow for arbitrary values of R/λ , our approach is based on Mie scattering, implemented in terms of Debye potentials and on Wigner rotations to build the desired scattering problem from the standard case of axial incidence.

We start by writing the electric field corresponding to the superposition of two incident plane waves propagating in the nonmagnetic and nonabsorbing host medium:

$$\mathbf{E}_{\text{in}}(\mathbf{r}, t) = \sum_{j=1}^2 E_0 \hat{\mathbf{e}}_j e^{i(\mathbf{k}_j \cdot \mathbf{r} - \omega t)}, \quad (1)$$

where the polarization unit vectors ($j = 1, 2$) are

$$\hat{\mathbf{e}}_j(\theta_j, \phi_j) = \cos \phi_j \hat{\boldsymbol{\theta}}_j - \sin \phi_j \hat{\boldsymbol{\phi}}_j. \quad (2)$$

The wave vectors

$$\mathbf{k}_j = n_h \frac{\omega}{c} (\sin \theta_j \cos \phi_j, \sin \theta_j \sin \phi_j, \cos \phi_j)$$

are written in terms of the speed of light in vacuum c and of the host-medium refractive index $n_h = \sqrt{\epsilon_h}$, where ϵ_h is the relative permittivity. The spherical polar and azimuthal angles

θ_j and ϕ_j define the propagation directions with respect to the z axis. When discussing specific examples, we will take $\phi_1 = 0$ and $\phi_2 = \pi$ for TM and $\phi_1 = \pi/2$ and $\phi_2 = 3\pi/2$ for TE polarization, as depicted in Fig. 1.

We introduce the electric (E) and magnetic (M) Debye potentials [41,42]

$$\Pi^E(\mathbf{r}) = \sum_{\ell=1}^{\infty} \frac{(\mathbf{r} \cdot \mathbf{E})}{\ell(\ell+1)}, \quad (3)$$

$$\Pi^M(\mathbf{r}) = \sum_{\ell=1}^{\infty} \frac{(\mathbf{r} \cdot \mathbf{H})}{\ell(\ell+1)}. \quad (4)$$

The electric and magnetic fields can be written in terms of the Debye potentials as follows:

$$\mathbf{E} = \nabla \times \nabla \times (\mathbf{r} \Pi^E) + i\omega\mu_0 \nabla \times (\mathbf{r} \Pi^M), \quad (5)$$

$$\mathbf{H} = \nabla \times \nabla \times (\mathbf{r} \Pi^M) - i\omega\epsilon_h\epsilon_0 \nabla \times (\mathbf{r} \Pi^E), \quad (6)$$

where ϵ_0 and μ_0 are the vacuum permittivity and permeability, respectively.

In order to derive the Debye potentials for a given plane wave, we first consider a “primed” coordinate system such that the z' and x' axes coincide with the propagation and polarization directions, respectively. In such a system, we find (omitting the time dependence from now on)

$$\hat{\mathbf{r}} \cdot \mathbf{E}(r, \theta', \phi') = E_0 e^{ikr \cos \theta'} \sin \theta' \cos \phi'. \quad (7)$$

The Debye potentials of a plane wave in the primed coordinate system are then obtained from Eqs. (3), (4), and (7) by expanding $e^{ikr \cos \theta'}$ in terms of spherical waves:

$$\begin{aligned} \Pi_{\text{pw}}^E(r, \theta', \phi') &= \frac{E_0}{k} \sum_{\ell=1}^{\infty} i^{\ell+1} \sqrt{\frac{\pi(2\ell+1)}{\ell(\ell+1)}} j_{\ell}(kr) \\ &\times [Y_{\ell,+1}(\theta', \phi') - Y_{\ell,-1}(\theta', \phi')], \end{aligned} \quad (8)$$

$$\begin{aligned} \Pi_{\text{pw}}^M(r, \theta', \phi') &= \frac{H_0}{k} \sum_{\ell=1}^{\infty} i^{\ell} \sqrt{\frac{\pi(2\ell+1)}{\ell(\ell+1)}} j_{\ell}(kr) \\ &\times [Y_{\ell,+1}(\theta', \phi') + Y_{\ell,-1}(\theta', \phi')], \end{aligned} \quad (9)$$

where $H_0 = \sqrt{\epsilon_h \epsilon_0 / \mu_0} E_0$ and j_{ℓ} and $Y_{\ell,m}$ denote the spherical Bessel functions and the spherical harmonics, respectively [43].

To describe an incident plane wave propagating along a generic direction defined by the spherical angles θ_j and ϕ_j , we implement a rotation from the primed to the unprimed coordinate system with the help of the Wigner rotation matrix elements $d_{m,\pm 1}^{\ell}(\theta_j)$ [44]. We then derive the Debye potentials for the incident field by taking a superposition of the plane-wave potentials (8) and (9) as in Eq. (1). The explicit expressions are written as sums over ℓ (for the total angular momentum J^2) and m (corresponding to J_z) of the form

$$\sum_{\ell,m} \equiv \sum_{\ell=1}^{\infty} \sum_{m=-\ell}^{\ell}.$$

We find

$$\Pi_{\text{in}}^E(r, \theta, \phi) = i \frac{E_0}{k} \sum_{\ell, m} \gamma_{\ell, m}^E j_\ell(kr) Y_{\ell, m}(\theta, \phi), \quad (10)$$

$$\Pi_{\text{in}}^M(r, \theta, \phi) = \frac{H_0}{k} \sum_{\ell, m} \gamma_{\ell, m}^M j_\ell(kr) Y_{\ell, m}(\theta, \phi). \quad (11)$$

The multipole coefficients $\gamma_{\ell, m}^{E, M}$ are written as a sum over the plane waves $j = 1, 2$ and the photon helicity $\varepsilon = \pm 1$:

$$\gamma_{\ell m}^{E, M} = \sqrt{\frac{\pi(2\ell+1)}{\ell(\ell+1)}} i^\ell \sum_{j, \varepsilon} g^{E, M}(\varepsilon) e^{-i\phi_j(m-\varepsilon)} d_{m, \varepsilon}^\ell(\theta_j), \quad (12)$$

with $g^E(\varepsilon) = \varepsilon$ and $g^M(\varepsilon) = 1$.

As we consider spherically symmetric particles, it is straightforward to obtain the Debye potentials for the scattered field \mathbf{E}_s by following the prescription outlined above:

$$\Pi_s^E(r, \theta, \phi) = i \frac{E_0}{k} \sum_{\ell, m} (-a_\ell) \gamma_{\ell, m}^E h_\ell^{(1)}(kr) Y_{\ell, m}(\theta, \phi), \quad (13)$$

$$\Pi_s^M(r, \theta, \phi) = \frac{H_0}{k} \sum_{\ell, m} (-b_\ell) \gamma_{\ell, m}^M h_\ell^{(1)}(kr) Y_{\ell, m}(\theta, \phi), \quad (14)$$

where $h_\ell^{(1)}(kr)$ are the spherical Hankel functions of the first kind [43]. The Mie coefficients a_ℓ and b_ℓ denote the scattering amplitudes for electric and magnetic multipoles, respectively. For a homogeneous dielectric sphere embedded in a nonabsorbing and nonmagnetic host medium, they are given by [45]

$$a_\ell = \frac{n_s \psi_\ell(n_s x) \psi'_\ell(x) - \mu_s \psi_\ell(x) \psi'_\ell(n_s x)}{n_s \psi_\ell(n_s x) \xi'_\ell(x) - \mu_s \xi_\ell(x) \psi'_\ell(n_s x)}, \quad (15)$$

$$b_\ell = \frac{\mu_s \psi_\ell(n_s x) \psi'_\ell(x) - n_s \psi_\ell(x) \psi'_\ell(n_s x)}{\mu_s \psi_\ell(n_s x) \xi'_\ell(x) - n_s \xi_\ell(x) \psi'_\ell(n_s x)}, \quad (16)$$

where $x = kR$ is the size parameter, n_s is the relative refractive index of the sphere with respect to the host medium, μ_s is the relative magnetic permeability of the sphere, and ψ_ℓ and ξ_ℓ are the Riccati-Bessel functions [43].

Once the total field $\mathbf{E} = \mathbf{E}_{\text{in}} + \mathbf{E}_s$ is known in terms of the Debye potentials for the incident and scattered fields, we are able to obtain the optical force acting upon the dielectric sphere by integration of the Maxwell stress tensor over a spherical surface at infinity:

$$\mathbf{F} = \lim_{r \rightarrow \infty} \left[-\frac{r}{2} \int \mathbf{r} (\epsilon_h \epsilon_0 E^2 + \mu_0 H^2) d\Omega \right]. \quad (17)$$

We choose our coordinate system with the z axis bisecting the propagation directions as shown in Fig. 1: $\theta_1 = \theta_2 = \Theta$, where 2Θ is the angle between the two propagation directions. As the two plane waves have equal amplitudes and the same polarization, the optical force points along the z direction by symmetry. F_z has two distinct contributions: the extinction term F_e arises from cross terms of the form $\mathbf{E}_{\text{in}} \cdot \mathbf{E}_s^*$ (and likewise for the magnetic field) and represents the rate of linear momentum removal from the incident fields. Not all of this momentum is transferred to the particle, as part of it is carried away by the scattered fields. Thus, the second contribution to the optical force F_s , which is quadratic in \mathbf{E}_s and \mathbf{H}_s , represents the negative of the rate of momentum

contained in the scattered electromagnetic fields. We find

$$F_z = F_s + F_e. \quad (18)$$

The scattering contribution is obtained by writing \mathbf{E}_s and \mathbf{H}_s in terms of the Debye potentials as in Eqs. (5) and (6), respectively, and then taking the asymptotic approximation of the Hankel functions in (13) and (14) when evaluating the Maxwell stress tensor surface integral (17):

$$F_s = \frac{\epsilon_h \epsilon_0 E_0^2}{k^2} \sum_{\ell, m} \text{Im} \left\{ \ell(\ell+2) \sqrt{\frac{(\ell+1-m)(\ell+1+m)}{(2\ell+1)(2\ell+3)}} \right. \\ \left. \times [a_\ell a_{\ell+1}^* \gamma_{\ell, m}^E \gamma_{\ell+1, m}^{E*} + b_\ell b_{\ell+1}^* \gamma_{\ell, m}^M \gamma_{\ell+1, m}^{M*}] - im b_\ell a_\ell^* \gamma_{\ell, m}^M \gamma_{\ell, m}^{E*} \right\}. \quad (19)$$

The extinction term results from interference between the incident and scattered fields and reads

$$F_e = \frac{\sqrt{\pi} \epsilon_h \epsilon_0 E_0^2}{2k^2} \sum_{\ell, m} \sum_{\varepsilon = \pm 1} \varepsilon \sqrt{\ell(\ell+1)(2\ell+1)} \\ \times \text{Re} [(a_\ell^* \gamma_{\ell, m}^{E*} + \varepsilon b_\ell^* \gamma_{\ell, m}^{M*}) G_{\ell, m}^\varepsilon]. \quad (20)$$

Equation (20) contains an additional sum over the photon helicity $\varepsilon = \pm 1$ and the associated coefficients

$$G_{\ell, m}^\varepsilon = i^\ell \sum_{j=1}^2 \cos \Theta d_{m, \varepsilon}^\ell(\Theta) e^{-i(m-\varepsilon)\phi_j}.$$

Dipolar limit. In order to gain a more physical insight, we compare the limiting values of our exact analytical expressions when $kR \ll 1$ with the known results for the force on an induced dipole. Within the dipolar approximation, the electromagnetic response is entirely captured by the induction of electric and magnetic dipoles: $\mathbf{p} = \epsilon_0 \alpha_e \mathbf{E}$ and $\mathbf{m} = \alpha_m \mathbf{H}$, where α_e and α_m denote the electric and magnetic polarizabilities, respectively.

Such a model is obtained as a limiting case of Mie scattering for very small spheres, $kR \ll 1$, as long as the sphere is magnetic or provided that the sphere refractive index is high enough to satisfy the additional condition $n_s kR \gg 1$ [45]. In such cases, the leading contribution in the extinction term (20) arises from both electric and magnetic dipole terms $\ell = 1$. The corresponding Mie coefficients are related to the electric and magnetic polarizabilities as follows:

$$a_1 = -i \frac{k^3}{6\pi} \alpha_e, \quad b_1 = -i \frac{k^3}{6\pi} \alpha_m. \quad (21)$$

Clearly, the extinction term (20) cannot provide a pulling contribution as the total momentum removed from the incident waves points along the positive z axis in Fig. 1. Indeed, the pulling force necessarily arises from the scattered field carrying an excess linear momentum along the positive z axis. Such an effect is captured by the scattering contribution (19), whose leading-order term is proportional to $b_1 a_1^*$, representing the coherent interference between electric and magnetic dipoles [33]. Together with the leading-order extinction terms,

they lead to the dipolar force

$$F_z \approx 2k\epsilon_h\epsilon_0 E_0^2 \left[\text{Im} \left(\frac{\alpha_e \cos \Theta}{\epsilon_h} + \alpha_m \cos^3 \Theta \right) - \frac{2k^3}{3\epsilon_h} \text{Re}(\alpha_e \alpha_m^*) \cos \Theta \right] \quad (22)$$

in the case of TE-polarized waves and to

$$F_z \approx 2k\epsilon_h\epsilon_0 E_0^2 \left[\text{Im} \left(\frac{\alpha_e \cos^3 \Theta}{\epsilon_h} + \alpha_m \cos \Theta \right) - \frac{2k^3}{3\epsilon_h} \text{Re}(\alpha_e \alpha_m^*) \cos \Theta \right] \quad (23)$$

in the case of TM polarization. Such expressions are obtained by neglecting the quadrupole and higher multipoles ($\ell \geq 2$) in (19) and (20) and using the explicit form of the Wigner matrix elements $d_{m,\pm 1}^1(\Theta)$. They agree with known results [33,34] for the dipolar regime.

In the case of very small nonmagnetic microspheres with moderate refractive indexes, the magnetic dipole turns out to be much smaller than the electric dipole and actually comparable to the electric quadrupole term associated with a_2 (Rayleigh scattering regime) [45]. Thus, OPF cannot be achieved in the Rayleigh limit, as the electric-magnetic dipole interference term appearing in (22) and (23) would be missing.

In the next section, we discuss in more detail the validity of the dipolar approximation by comparing the full evaluation of the Mie series expressions (19) and (20) with the approximations (22) and (23) consisting of keeping only the dipolar terms involving a_1 and b_1 . We will confirm that the dipolar approximation is more accurate for higher refractive indexes. As expected, this is also the case allowing us to achieve OPF with smaller particles.

III. RESULTS AND DISCUSSION

For the numerical examples discussed in this section, we take the vacuum wavelength to be $\lambda_0 = 1064$ nm. For the host medium, we consider an aqueous solution with $n_h = 1.332$. We normalize the optical force to $F_0 = 2\pi n_h I_0 / (k^2 c)$, where $I_0 = \sqrt{\epsilon_h \epsilon_0 / \mu_0} E_0^2 / 2$ is the intensity of each incident plane wave shown in Fig. 1.

In Fig. 2, we compare the exact results for the optical force (solid line), calculated from Eqs. (18), (19), and (20), with the dipolar approximations (22) and (23) (dashed line). For the latter, the polarizabilities are calculated from (21) by taking the full exact expressions for the Mie coefficients a_1 and b_1 .

In Figs. 2(a) and 2(b), we consider a silicon sphere (refractive index of 3.5) of radius $R = 140$ nm and plot the axial force as a function of the half angle Θ between the two incident wave vectors, as shown in Figs. 1(a) and 1(b) for TE and TM polarizations, respectively. Figures 2(a) and 2(b) show that the dipolar approximation is capable of reproducing the features of the exact curve in this example with a small sphere and high refractive index. OPF is achieved in the interval $65^\circ < \Theta < 90^\circ$ only in the case of TE polarization and is explained by the coherent interference between electric and magnetic dipoles, as discussed in connection with Eq. (22).

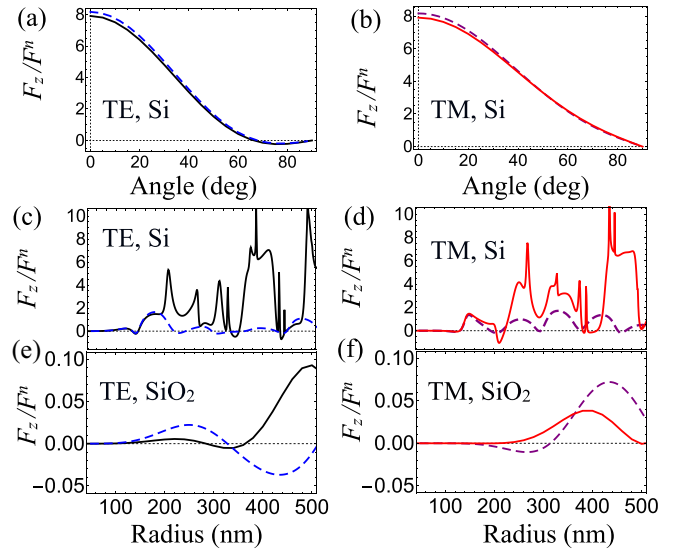


FIG. 2. Normalized optical force acting on Si or SiO₂ microspheres under illumination by two plane waves with the same intensity and linear polarization. All panels show the result of the full Mie calculation (solid lines) and of the dipolar approximation (dashed lines). The polarization is TE in (a), (c), and (e) and TM in (b), (d), and (f) (see Fig. 1). (a) and (b) Optical force as a function of the half angle Θ for Si microspheres of radius 140 nm. (c) and (d) for Si and (e) and (f) for SiO₂ show the optical force as a function of sphere radius for $\Theta = 78^\circ$.

The maximum pulling force occurs at $\Theta = 78^\circ$. In Figs. 2(c)–2(e) we fix the incident angle at $\Theta = 78^\circ$ and plot the force as a function of the sphere radius R . Figures 2(c) and 2(d) correspond to Si microspheres, whereas Figs. 2(e) and 2(f) show the results for SiO₂ microspheres, with refractive index $n_{\text{SiO}_2} = 1.45$. The polarization is TE in Figs. 2(c) and 2(e) and TM in Figs. 2(d) and 2(f).

In the case of silicon, OPF is also achieved for TM polarization, as shown in Fig. 2(d). In contrast to the TE configuration, the pulling effect here is not captured by the dipolar curve and is then not related to interference between electric and magnetic dipoles. Instead, it results from contributions of higher multipoles yielding an enhancement of scattering along the z axis bisecting the directions of incidence which can be understood only within the full Mie theory as it takes place at larger radii.

As expected, the dipolar approximation fails to describe the behavior of the optical force on SiO₂ microspheres in the size range shown in Figs. 2(e) and 2(f). Since its refractive index is lower than in the case of silicon, very small SiO₂ spheres behave as induced electric dipoles with a negligible magnetic dipole contribution. As a consequence, the exact optical force is mostly positive in the range shown in Figs. 2(e) and 2(f) (except for a negligible pulling effect near $R \sim 320$ nm for TE polarization). In short, OPF is not found in the case of very small SiO₂ beads as the scattering angular distribution resembles the electric dipole (Rayleigh) distribution and hence does not favor the forward direction.

To circumvent this issue we put forward the strategy of doping the SiO₂ spheres with gold spherical inclusions (radius a) in order to excite electric and magnetic dipoles simultane-

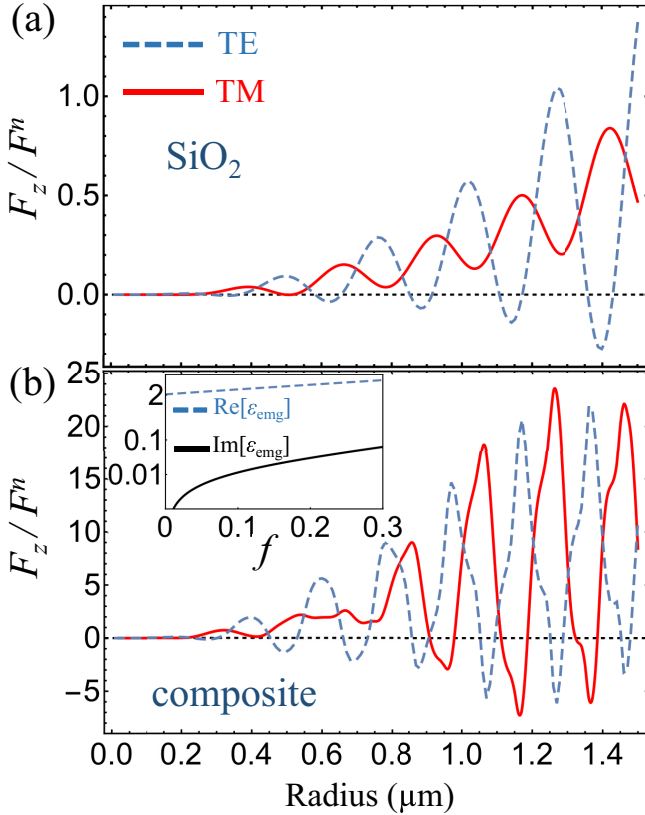


FIG. 3. Normalized optical force as a function of sphere radius for (a) homogeneous SiO_2 microspheres and (b) composite SiO_2 microspheres with gold inclusions (filling fraction $f = 0.18$). The incident plane waves are either TE (dashed lines) or TM (solid lines) polarized. The half angle between the incidence directions is $\Theta = 85^\circ$. The inset shows the real (dashed line) and imaginary (solid line) parts of the composite effective permittivity ϵ_{emg} as a function of the filling fraction.

ously. We assume $a \ll \lambda$ and then model this system as an effectively homogeneous medium with the help of the extended Maxwell-Garnet theory [46,47]. The effective refractive index of the composite sphere $n_{\text{eff}} = \sqrt{\epsilon_{\text{emg}}\mu_{\text{emg}}}$ is obtained from the effective relative permittivity and permeability:

$$\epsilon_{\text{emg}} = \epsilon_h \frac{x_i^3 + 3ifa_1^i}{x_i^3 - \frac{3}{2}ifa_1^i}, \quad (24)$$

$$\mu_{\text{emg}} = \frac{x_i^3 + 3ifb_1^i}{x_i^3 - \frac{3}{2}ifb_1^i}, \quad (25)$$

where f denotes the volume filling fraction. The dipolar Mie coefficients of the inclusions a_1^i and b_1^i are derived from the corresponding size parameter $x_i = n_{\text{SiO}_2}\omega a/c$ and from the value $\epsilon_{\text{Au}} = -48.45 + 3.6i$ for the gold relative permittivity at $\lambda_0 = 1064 \text{ nm}$ [48].

In Fig. 3, we plot the optical force as a function of sphere radius R for TE (dashed) and TM (solid) polarizations. We take $\Theta = 85^\circ$ as the half angle between the two beams. The results for homogeneous SiO_2 spheres ($f = 0$) are shown in Fig. 3(a), whereas the force on composite spheres with gold inclusions ($f = 0.18$) is shown in Fig. 3(b). Measurable OPF

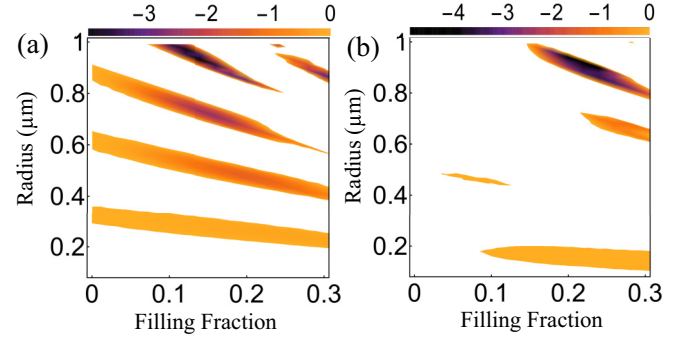


FIG. 4. Optical pulling force on a composite microsphere as a function of radius and filling fraction. For clarity, only regions in the parameter space leading to pulling forces are shown. (a) TE and (b) TM polarization. The half angle between the incidence directions is fixed at $\Theta = 85^\circ$.

on homogeneous SiO_2 spheres can be obtained for relatively large radii in the case of TE polarization, while the force is always positive for TM. Such a striking difference between the two cases shows that the relative phase between the scattered fields produced by each plane-wave component strongly depends on the incident polarization. Thus, the condition for constructive interference near the forward direction can be controlled by the incident polarization.

The scenario is drastically changed when one considers the SiO_2 host sphere with gold inclusions, as shown in Fig. 3(b). Indeed, the presence of gold inclusions not only allows for OPF for both TE and TM polarizations but also increases its magnitude by about one order of magnitude. At specific size ranges and depending on the polarization, the fields scattered by the inclusions interfere constructively (destructively) near the forward (backward) direction, then leading to a strong pulling effect. The resulting optical forces for TE and TM polarizations oscillate nearly out of phase as a function of the radius, as shown in Fig. 3(b). Thus, the size intervals allowing for OPF using TE beams is approximately the complement of the intervals allowing for OPF using TM beams. Such a feature indicates the possibility of a polarization-controlled particle sorting according to particle size.

Adding metallic inclusions also allows us to extend the range of optical pulling towards smaller sizes. Indeed, the effective permittivity ϵ_{emg} increases with the filling fraction f , as shown in the inset of Fig. 3(b). Moreover, the inclusions also lead to an effective permeability μ_{emg} slightly different from the one according to Eq. (25). In line with the discussion in Sec. II, both effects enhance the magnetic dipole contribution, which is essential for achieving OPF on small particles.

The occurrence of OPF on small particles is better visualized in the density plot of the OPF versus sphere radius and filling fraction shown in Figs. 4(a) and 4(b) for TE and TM polarizations, respectively. Colored areas indicate optical pulling forces, whereas the regions corresponding to optical pushing forces are left blank for clarity. The overall disposition of the colored regions indicate that the conditions for OPF become more selective for bigger particles as a larger number of multipoles contribute to scattering. Indeed, in this case a fine tuning of the material parameters is required to

achieve the simultaneous interferometric conditions involving all multipoles contributing to the scattering force component (19).

In the case of TE polarization, the colored areas appear as a pattern of stripes illustrating how the size intervals allowing for OPF depend on the filling fraction. Within a given stripe, the magnitude of the OPF is initially enhanced as f increases from zero (homogeneous case). Stripes corresponding to larger radii (upper part) are increasingly more inclined and tend to shrink as the filling fraction increases. Both features are related to light absorption by the microsphere. The inset of Fig. 3(b) shows that $\text{Im}(\epsilon_{\text{eff}})$ increases sharply as a function of f . As the penetration depth $\delta = \lambda_0/[4\pi \text{Im}(n_{\text{eff}})]$ decreases approaching the sphere diameter $2R$, the fraction of absorbed light increases, which is clearly detrimental to the pulling effect. For very small spheres, $R \ll \delta$, absorption is still negligible, and then the widths of the lower stripes in Fig. 4(a) are approximately uniform. On the other hand, the stripes corresponding to larger radii are more affected by absorption, as expected. They shrink and eventually disappear as f and, consequently, $\text{Im}(n_{\text{eff}})$ increase. Also, the inclination of the stripes shows that the reduction of the penetration depth δ is compensated by a sharp decrease in the radii, allowing for pulling to keep the ratio R/δ approximately unchanged.

The overall picture is similar in the case of TM polarization shown in Fig. 4(b). However, the pulling regions are more scarce, and very small filling fractions are excluded in this case.

IV. CONCLUSION

We have developed a theoretical framework to calculate the optical pulling force on a microsphere illuminated by a superposition of plane waves. Due to the rotational symmetry of the scatterer, Mie scattering of plane waves propagating along arbitrary directions can be connected with the more standard case of axial propagation by employing Wigner rotation ma-

trices and Debye potentials. We have derived an explicit result for the optical force as a partial-wave series when considering the example involving two linearly polarized plane waves. However, it is straightforward to extend our approach to multiple plane waves with arbitrary polarizations. The case of circular polarization might be particularly interesting given its possible application to enantioselective manipulation of chiral particles.

Our results show that TE-polarized waves can pull low- and high-refractive-index particles alike. In the former case, the technique is limited to larger sizes, involving higher multipoles beyond the electric and magnetic dipoles. On the other hand, TM-polarized waves allow for OPF only on high-refractive-index particles. We have shown that the use of a metamaterial platform not only leads to an order of magnitude increase in the pulling force but also allows us to pull smaller particles, thus extending the technique into the dipolar regime. As a specific example, we have considered a low-index dielectric sphere doped with plasmonic inclusions. The strong enhancement in the pulling force is achieved for small values of the filling fraction to avoid the detrimental effect of absorption. In this configuration, the size ranges which allow for pulling for each orthogonal polarization are approximately complementary. Such a feature could be applied to implement a polarization-controlled particle sorting using OPF.

ACKNOWLEDGMENTS

Funding was provided by the National Council for Scientific and Technological Development (CNPq-Brazil), the Coordination for the Improvement of Higher Education Personnel (CAPES-Brazil), the National Institute of Science and Technology Complex Fluids (INCT-FCx), and the research foundations of the states of Minas Gerais (FAPEMIG), Rio de Janeiro (FAPERJ), and São Paulo (FAPESP). We thank F. S. S. da Rosa and S. Iqbal for inspiring discussions.

-
- [1] A. Ashkin, Acceleration and Trapping of Particles by Radiation Pressure, *Phys. Rev. Lett.* **24**, 156 (1970).
 - [2] A. Ashkin, J. M. Dziedzic, J. E. Bjorkholm, and S. Chu, Observation of a single-beam gradient force optical trap for dielectric particles, *Opt. Lett.* **11**, 288 (1986).
 - [3] A. Ashkin, *Optical Trapping and Manipulation of Neutral Particles Using Lasers: A Reprint Volume with Commentaries* (World Scientific, Singapore, 2006).
 - [4] J. Gieseler, J. R. Gomez-Solano, A. Magazzù, I. P. Castillo, L. P. García, M. Gironella-Torrent, X. Viader-Godoy, F. Ritort, G. Pesce, A. V. Arzola, K. Volke-Sepulveda, and G. Volpe, Optical tweezers: A comprehensive tutorial from calibration to applications, [arXiv:2004.05246](https://arxiv.org/abs/2004.05246).
 - [5] M. E. J. Friese, T. A. Nieminen, N. R. Heckenberg, and H. Rubinsztein-Dunlop, Optical alignment and spinning of laser-trapped microscopic particles, *Nature (London)* **394**, 348 (1998).
 - [6] D. G. Grier, A revolution in optical manipulation, *Nature (London)* **424**, 810 (2003).
 - [7] J. Lin and Y. Q. Li, Optical trapping and rotation of airborne absorbing particles with a single focused laser beam, *Appl. Phys. Lett.* **104**, 101909 (2014).
 - [8] K. Diniz, R. S. Dutra, L. B. Pires, N. B. Viana, H. M. Nussenzweig, and P. A. Maia Neto, Negative optical torque on a microsphere in optical tweezers, *Opt. Express* **27**, 5905 (2019).
 - [9] R. Ali, F. A. Pinheiro, F. S. S. Rosa, R. S. Dutra, P. A. Maia Neto, Enantioselective manipulation of chiral nanoparticles using optical tweezers, *Nanoscale* **12**, 5031 (2020).
 - [10] F. M. Fazal and S. M. Block, Optical tweezers study life under tension, *Nat. Photonics* **5**, 318 (2011).
 - [11] O. M. Maragò, P. H. Jones, P. G. Gucciardi, G. Volpe, and A. C. Ferrari, Optical trapping and manipulation of nanostructures, *Nat. Nanotechnol.* **8**, 807 (2013).
 - [12] O. Brzobohaty, M. Siler, J. Trojek, L. Chvatal, V. Karasek, A. Patak, Z. Pokorna, F. Mika, and P. Zemanek, Three-dimensional optical trapping of a plasmonic nanoparticle using low numerical aperture optical tweezers, *Sci. Rep.* **5**, 8106 (2015).

- [13] P. Polimeno, A. Magazzù, M. A. Iatì, F. Patti, R. Saija, C. D. E. Boschi, M. G. Donato, P. G. Gucciardi, P. H. Jones, G. Volpe, and O. M. Maragò, Optical tweezers and their applications, *J. Quantum Spectrosc. Radiat. Transfer* **218**, 131 (2018).
- [14] S. H. Lee, Y. Roichman, and D. G. Grier, Optical solenoid beams, *Opt. Express* **18**, 6988 (2010).
- [15] J. Chen, J. Ng, Z. F. Lin, and C. T. Chan, Optical pulling force, *Nat. Photonics* **5**, 531 (2011).
- [16] X. Li, J. Chen, Z. Lin, and J. Ng, Optical pulling at macroscopic distances, *Sci. Adv.* **5**, 7814 (2019).
- [17] V. Shvedov, A. R. Davoyan, N. Engheta, and W. Krolikowski, A long-range polarization-controlled optical tractor beam, *Nat. Photonics* **8**, 846 (2014).
- [18] H. Chen, S. Liu, J. Zi, and Z. Lin, Fano resonance-induced negative optical scattering force on plasmonic nanoparticles, *ACS Nano* **9**, 1926 (2015).
- [19] T. Zhu, Y. Cao, L. Wang, Z. Nie, T. Cao, F. Sun, Z. Jiang, M. Nieto-Vesperinas, Y. Liu, C.-W. Qiu, and W. Ding, Self-Induced Backaction Optical Pulling Force, *Phys. Rev. Lett.* **120**, 123901 (2018).
- [20] R. W. Bowman and M. J. Padgett, Optical trapping and binding, *Rep. Prog. Phys.* **76**, 026401 (2013).
- [21] M. Mazilu and K. Dholakia, Resonance enhanced optical manipulation: The push and pull of light, *Proc. SPIE* **8458**, 845809 (2012).
- [22] O. Brzobohaty, V. Karasek, M. Siler, L. Chvatal, T. Cizmar, and P. Zemanek, Experimental demonstration of optical transport, sorting and self-arrangement using a ‘tractor beam,’ *Nat. Photonics* **7**, 123 (2013).
- [23] G. S. Wiederhecker, L. Chen, A. Gondarenko and M. Lipson, Controlling photonic structures using optical forces, *Nature (London)* **462**, 633 (2009).
- [24] A. Canaguier-Durand, J. A. Hutchison, C. Genet, and T. W. Ebbesen, Mechanical separation of chiral dipoles by chiral light, *New J. Phys.* **15**, 123037 (2013).
- [25] K. Ding, J. Ng, L. Zhou, and C. T. Chan, Realization of optical pulling forces using chirality, *Phys. Rev. A* **89**, 063825 (2014).
- [26] D. S. Bradshaw and D. L. Andrews, Chiral discrimination in optical trapping and manipulation, *New J. Phys.* **16**, 103021 (2014).
- [27] S. B. Wang and C. T. Chan, Lateral optical force on chiral particles near a surface, *Nat. Commun.* **5**, 3307 (2014).
- [28] A. Hayat, J. B. Mueller, and F. Capasso, Lateral chirality-sorting optical forces, *Proc. Natl. Acad. Sci. USA* **112**, 13190 (2015).
- [29] M. Kamandi, M. Albooyeh, C. Guclu, M. Veysi, J. Zeng, K. Wickramasinghe, and F. Capolino, Enantiospecific Detection of Chiral Nanosamples using Photoinduced Force, *Phys. Rev. Appl.* **8**, 064010 (2017).
- [30] W. Ding, T. Zhu, L. M. Zhou, and C. W. Qiu, Photonic tractor beams: A review, *Adv. Photonics* **1**, 024001 (2019).
- [31] F. G. Mitri, R. X. Li, R. P. Yang, L. X. Guo, and C. Y. Ding, Optical pulling force on a magneto-dielectric Rayleigh sphere in Bessel tractor polarized beams, *J. Quantum Spectrosc. Radiat. Transfer* **184**, 360 (2016).
- [32] I. V. Krasnov, Bichromatic optical tractor beam for resonant atoms, *Phys. Lett. A* **376**, 2743 (2012).
- [33] H. Liu, M. Panmai, Y. Peng, and S. Lan, Optical pulling and pushing forces exerted on silicon nanospheres with strong coherent interaction between electric and magnetic resonances, *Opt. Express* **11**, 12357 (2017).
- [34] E. Mobini, A. Rahimzadegan, C. Rockstuhl, and R. Alaei, Theory of optical forces on small particles by multiple plane waves, *J. Appl. Phys.* **124**, 173102 (2018).
- [35] X. Bian, D. L. Gao, and L. Gao, Tailoring optical pulling force on gain coated nanoparticles with nonlocal effective medium theory, *Opt. Express* **25**, 24566 (2017).
- [36] R. Alaei, J. Christensen, and M. Kadic, Optical Pulling and Pushing Forces in Bilayer \mathcal{PT} -Symmetric Structures, *Phys. Rev. Appl.* **9**, 014007 (2018).
- [37] S. Sukhov and A. Dogariu, Negative Nonconservative Forces: Optical Tractor Beams for Arbitrary Objects, *Phys. Rev. Lett.* **107**, 203602 (2011).
- [38] N. O. Länk, P. Johansson, and M. Käll, Directional scattering and multipolar contributions to optical forces on silicon nanoparticles in focused laser beams, *Opt. Express* **26**, 29074 (2018).
- [39] R. Ali, F. A. Pinheiro, F. S. S. Rosa, R. S. Dutra, and P. A. M. Neto, Optimizing optical tweezing with directional scattering in composite microspheres, *Phys. Rev. A* **98**, 053804 (2018).
- [40] R. Ali, Revisit of generalized Kerker’s conditions using composite metamaterials, *J. Optics* **22**, 085102 (2020).
- [41] C. J. Bouwkamp and H. B. G. Casimir, On multipole expansions in the theory of electromagnetic radiation, *Physica* **20**, 539 (1954).
- [42] P. A. Bobbert, and J. Vlioger, Light scattering by a sphere on a substrate, *Phys. A (Amsterdam, Neth.)* **137**, 209 (1986).
- [43] NIST Digital Library of Mathematical Functions, release 1.0.27, edited by F. W. J. Olver, A. B. Olde Daalhuis, D. W. Lozier, B. I. Schneider, R. F. Boisvert, C. W. Clark, B. R. Miller, B. V. Saunders, H. S. Cohl, and M. A. McClain, <http://dlmf.nist.gov/>.
- [44] A. R. Edmonds, *Angular Momentum in Quantum Mechanics* (Princeton University Press, Princeton, NJ, 1957).
- [45] C. F. Bohren and D. R. Huffman, *Absorption and Scattering of Light by Small Particles* (Wiley, New York, 1983).
- [46] R. Ruppin, Evaluation of extended Maxwell-Garnett theories, *Opt. Commun.* **182**, 273 (2000).
- [47] P. Mallet, C. A. Guerin and A. Sentenac, Maxwell-Garnett mixing rule in the presence of multiple scattering: Derivation and accuracy, *Phys. Rev. B* **72**, 014205 (2005).
- [48] P. B. Johnson and R. W. Christy, Optical constants of the noble metals, *Phys. Rev. B* **6**, 4370 (1972).